fermentation

MDPI

Article

Evaluating the Performance of *Yarrowia lipolytica* 2.2ab in Solid-State Fermentation under Bench-Scale Conditions in a Packed-Tray Bioreactor

Alejandro Barrios-Nolasco [1,2], Carlos Omar Castillo-Araiza [3,*], Sergio Huerta-Ochoa [1], María Isabel Reyes-Arreozola [4], José Juan Buenrostro-Figueroa [1,5] and Lilia Arely Prado-Barragán [1,*]

1 Solid Fermentations Pilot Plant, Biotechnology Department, Universidad Autónoma Metropolitana–Iztapalapa, Av. San Rafael Atlixco 186, Col. Vicentina, Ciudad de México 09340, Mexico; ing.alejandro.bn@gmail.com (A.B.-N.); sho@xanum.uam.mx (S.H.-O.); jose.buenrostro@ciad.mx (J.J.B.-F.)
2 Laboratory of Cell Biology and Natural Products, National School of Homeopathy, National Polytechnic Institute, Guillermo Massieu Helguera, Ciudad de México 07320, Mexico
3 Laboratory of Catalytic Reactor Engineering Applied to Chemical and Biological Systems (LCRE), Department of Process Engineering and Hydraulics, Universidad Autónoma Metropolitana-Iztapalapa, Ciudad de México 09340, Mexico
4 Food Industries Department, National Technological Institute, Higher Technological Institute of the East of the State of Hidalgo, Carretera Apan-Tepeapulco, Las Peñitas, Apan 43900, Mexico; mireyes@itesa.edu.mx
5 Center for Research in Food and Development, Av. Cuarta Sur 3820, Fracc. Vencedores del Desierto, Chihuahua 33089, Mexico
* Correspondence: coca@xanum.uam.mx (C.O.C.-A.); lapb@xanum.uam.mx (L.A.P.-B.)

Abstract: Solid-State Fermentation (SSF) offers a valuable process for converting agri-food by-products (AFBP) into high-value metabolites, with *Yarrowia lipolytica* 2.2ab (*Yl*2.2ab) showing significant potential under laboratory-scale controlled conditions; however, its assessment in larger-scale bioreactor scenarios is needed. This work evaluates *Yl*2.2ab's performance in a bench-scale custom-designed packed-tray bioreactor. Key features of this bioreactor design include a short packing length, a wall-cooling system, and forced aeration, enhancing hydrodynamics and heat and mass transfer within the tray. Preliminary studies under both abiotic and biotic conditions assessed *Yl*2.2ab's adaptability to extreme temperature variations. The results indicated effective oxygen transport but poor heat transfer within the tray bed, with *Yl*2.2ab leading to a maximum growth rate of 28.15 m_{gx} $g_{ssdb}{}^{-1}$ h^{-1} and maximum production of proteases of 40.10 U $g_{ssdb}{}^{-1}$ h^{-1}, even when temperatures at the packed-tray outlet were around 49 °C. Hybrid-based modeling, incorporating Computational Fluid Dynamics (CFD) and Pseudo-Continuous Simulations (PCSs), elucidated that the forced-aeration system successfully maintained necessary oxygen levels in the bed. However, the low thermal conductivity of AFBP posed challenges for heat transfer. The bioreactor design presents promising avenues for scaling up SSF to valorize AFBP using *Yl*2.2ab's extremophilic capabilities.

Keywords: *Yarrowia lipolytica* 2.2ab; solid-state fermentation; experimentation; modeling; agroindustrial by-products; protease production

Citation: Barrios-Nolasco, A.; Castillo-Araiza, C.O.; Huerta-Ochoa, S.; Reyes-Arreozola, M.I.; Buenrostro-Figueroa, J.J.; Prado-Barragán, L.A. Evaluating the Performance of *Yarrowia lipolytica* 2.2ab in Solid-State Fermentation under Bench-Scale Conditions in a Packed-Tray Bioreactor. *Fermentation* **2024**, *10*, 344. https://doi.org/10.3390/fermentation10070344

Academic Editor: Bartłomiej Zieniuk

Received: 13 April 2024
Revised: 27 June 2024
Accepted: 27 June 2024
Published: 29 June 2024

1. Introduction

Among non-conventional yeasts of industrial interest, *Yarrowia lipolytica* (*Yl*) is a dimorphic microorganism with a unique trait known as metabolic flexibility [1–4]. This flexibility enables *Yl* to utilize various carbon-based sources for its metabolism, including hydrophobic and agri-food waste-based substrates [1–4]. Its metabolic adaptability to these substrates, producing high-value metabolites such as proteases, biofuels, food additives, and therapeutic compounds, makes *Yl* a promising yeast for diverse industrial applications [1–7]. Among the possibilities for increasing the metabolic potential of *Yl*, Solid-State Fermentation (SSF) presents several technical advantages [1–10] due to its potential to

produce high yields of metabolites, and the risk of contamination is lower compared to other biotechnological processes such as Liquid-Based Fermentation (LBF). Additionally, SSF downstream processing is economically more attractive than LBF [4,8].

When agri-food by-products (AFBP) are used as a substrate for Solid State Fermentation (SSF) altogether with *Yl*, a properly designed bioreactor to ensure efficient metabolic production is required. Factors such as temperature, oxygen, and substrate moisture can significantly impact its metabolic activity [1–13]. Because of this, most experimental studies assessing the impact of *Yl* have been carried out under laboratory-scale controlled conditions where the effects of heat and mass transport on its metabolic activity present a minor impact [1–4]. Among these SSF laboratory-scale studies, *Yarrowia lipolytica* 2.2ab (*Yl*2.2ab) has shown significant potential for valorizing AFBP-based substrates to produce metabolites such as proteases, having optimal performance at temperatures around 45 °C [2,14]. This laboratory result makes *Yl*2.2ab a promising microorganism for study under larger-scale bioreactor conditions, where variations in temperature, oxygen concentration, and substrate moisture can drastically impact its metabolic performance.

Four types of bioreactor designs have been implemented for carrying out conventional or unconventional SSF using synthetic culture media or AFBP as substrate-based, respectively [8,14]. These designs can be classified as (i) reactors without both mixing and forced aeration, (ii) reactors without mixing and with forced aeration, (iii) reactors with mixing and without forced aeration, and (iv) reactors with both mixing and forced aeration. Among the promising conventional bioreactors, packed-bed and packed-tray bioreactors have shown to be effective technologies for scaling up SSF under conventional scenarios [10–12,14,15]. However, heat and mass transfer resistances have significantly impacted the performance of the microorganism, an aspect that is exacerbated when AFBP-based substrates are used [10–17]. To this end, studies of *Yl* under larger-scale scenarios in bioreactors based on packed-bed and packed-tray technologies are limited and need to be analyzed to assess its potential for larger-scale bioreactors. In particular, for *Yl*2.2ab, these studies need to be initiated to assess its performance under conditions that can elucidate its potential for industrial applications.

This work evaluates the performance of *Yl*2.2ab in a bench-scale custom-designed packed-tray bioreactor. The bioreactor design, A new system concept for the assessment of SSF, incorporates features of both tray and packed-bed bioreactors, including a low packing height, a wall-cooling system, and forced aeration, using an in-house oxygen dispersion system to enhance hydrodynamics and heat and mass transfer within the bioreaction zone [14,15]. Preliminary experimental and modeling studies under both abiotic and biotic conditions were carried out to shed light on the adaptability and effectiveness of *Yl*2.2ab in the growth and production of proteases under extreme temperature and moisture variations within the bioreaction zone. Hybrid modeling, which combined Computational Fluid Dynamics (CFD) and Pseudo-Continuous Simulations (PCSs), along with experimentation, elucidated the bioreactor's performance regarding fluid dynamics and heat and mass transport and their impact on *Yl*2.2ab growth and protease production. It is worth mentioning that this work, based on a novel bioreactor design, aims to guide future efforts associated with the scaling-up of SSF to valorize AFBP-based substrates using *Yl*2.2ab, which presents metabolic flexibility and extremophilic character, as elucidated throughout this research.

2. Materials and Methods

2.1. Microorganism

Lyophilized *Yl*2.2ab, from the collection of the solid-fermentation pilot plant of the Metropolitan Autonomous University [18], was suspended with 10 mL of a sterile 0.01% (*v/v*) Tween-80 solution. Then, 1 mL of the cell suspension was inoculated in an Erlenmeyer flask containing 30 mL of potato dextrose agar (PDA) and incubated at 45 °C for eight days. The cells were collected by adding 30 mL of a sterile 0.01% (*v/v*) Tween-80 solution and shaking them at medium speed with a magnetic stirrer on a shaking rack to detach the cells

from the agar surface. Finally, 500 µL of the cell solution was mixed in vials with 500 µL of a 30% (*v/v*) glycerol solution and sterilized glass beads to preserve the microorganism. The preserved strain was kept refrigerated at 4 °C until use.

2.2. Inoculum Preparation

Three to four glass beads were taken from the vials and placed in flasks with PDA. The flasks were incubated at 45 °C for 8 days. The cell culture medium was collected by adding 3 mL of a sterile 0.01% (*v/v*) Tween-80 solution and shaking it with a sterile magnetic bar. Then, a 100-µL suspension aliquot was taken and diluted to a ratio of 1:100 with sterile 0.01% (*v/v*) Tween-80 solution, and finally, the cells were counted in a Neubauer® (Marienfeld, Germany) chamber, with 1×10^9 cells per gram of solid support on a dry basis (cell $g_{ssdb}{}^{-1}$).

2.3. Solid Culture Medium (Fermentable Solid Mass)

The tray was packed with pellets of a solid culture-based medium previously treated and containing 46.7% of fruit and vegetable by-products and 53.3% of soybean paste. The fruit and vegetable by-products were dehydrated before their use and, along with the soybean paste, were ground to homogenize the pellet size (1.41–1.68 mm). The tray was packed with 400 g of the moisturized fermentable solid mass (fruit and vegetable by-products, also referred to as AFBP throughout the document, and soybean paste). The fermentable solid mass, before being packed in the bioreactor, was moisturized with 240 mL of the mineral salt solution containing ions and micronutrients (as described below) required for the growth and metabolism of *Yl*2.2ab and then inoculated with a solution of 1×10^9 cells $g_{ssdb}{}^{-1}$, with an initial moisture of 60% in the solid mass [2,14,18]. The tray (300 cm^2; 15 × 20 cm), packed with 400 g of the moisturized solid culture medium, was adjusted to have a packing height of 2 cm. SSF in the bench-scale packed-tray bioreactor was carried out with a cooling temperature of 45 °C for 72 h, supplying saturated air at a constant inlet flow rate of 300 mL min^{-1}. Note that the moisture, nutrients, and micronutrients contained in the fermentable solid mass, as well as the initial operational temperatures set in the bioreactor, were conditions determined in laboratory-based experimentation to optimize the performance of *Yl*2.2ab in terms of growth and production of proteases.

Mineral Salt Solution (Micronutrients)

The mineral salt solution was prepared with the following composition (g L^{-1}): 0.02 $(NH_4)_2SO_4$; 1.0 KH_2PO_4; 0.5 $MgSO_47H_2O$; 0.5 KCl; and 30 $C_6H_{12}O_6$. The salts were dissolved in a 0.2 M NaOH-NaH_2PO_4 buffer solution (pH of 12 and 5 mM $CaCl_2$) [2,14,19].

2.4. Chemical and Elemental Composition of the Solid Culture-Based Medium

Nitrogen content was determined by the Micro–Kjeldahl method [20], and total sugars were measured by the phenol-sulfuric method [21]. Water activity (a_w) was assessed with an AQUA Lab® CX2 system (Decagon, Pullman, WA, USA), and moisture content was measured with a Thermobalance (OHAUS®, Heuwinkelstrasse, Switzerland). Elemental analysis of total carbon (C), hydrogen (H), nitrogen (N), and oxygen (O) contents was performed using an Elemental Analyzer® (Perkin Elmer Series II CHNS/O Analyzer 2400, Waltham, MA, USA). The chemical and carbon-based elemental composition for protein ($CH_{1.94}O_{0.56}N_{0.27}$), fat ($CH_{1.84}O_{0.114}$), carbohydrate ($CH_2O$), and fiber ($CH_{1.67}O_{0.83}$) were determined for the fruits and vegetables ($CH_{2.08}O_{0.82}N_{0.035}$) and soybean paste ($CH_{1.85}O_{0.75}N_{0.144}$) packed in the bioreactor tray. Table 1 presents the chemical and elemental composition of the components of the solid culture-based medium.

Table 1. Chemical and elemental composition of the components of the solid culture-based medium (AFBP).

Component (%)	Fruits and Vegetables	Soy Paste
Moisture	5.09	6.91
Protein	7.43	34.56
Carbohydrates	73.04	52.01
Fat	2.02	1.36
Fiber	11.13	5.30
Ash	6.38	6.77
Element (%)		
C	66.72	44.20
H	11.58	6.83
N	2.80	7.43

2.5. Enzyme Extraction and Proteolytic Activity

To obtain the enzymatic extract, 20 mL of distilled water was used for every 6 g of fermented dough. The fermented material was shaken for 10 min and then centrifuged at 7000 rpm for 10 min. The precipitate was discarded, and the remaining liquid (supernatant) was used to determine the proteolytic activity.

Proteolytic activity in the extracts was determined using a modified version of the method reported in the literature [22]. A 1% casein solution was prepared in a 50 mM phosphate buffer solution (pH of 7) containing 50 mM $CaClCO_2$. For each assay, 100 µL of the enzyme extract was mixed with 900 µL of the casein solution. The reaction was carried out at 40 °C for 10 min, and then 1 mL of 5% trichloroacetic acid (TCA) at 4 °C was added to stop the reaction. The samples were centrifuged at 10,000 rpm for 10 min, and the precipitate was discarded. The supernatant was recovered and filtered through fine-pore filter paper (Per-Filter Grade 615, pore opening of 8 µm). Finally, the filtrate was read using a spectrophotometer at 280 nm. A control was prepared with 100 µL of enzyme extract and 900 µL of buffer solution, treated the same way as the samples. A tyrosine calibration curve (1 mg mL^{-1}) was used. One unit of protease activity was defined as the amount of enzyme necessary to release 1 µg of tyrosine per minute under the assay conditions.

2.6. Physical and Thermodynamic Properties of the Solid Culture-Based Medium

Some physical properties of the solid culture medium were determined using well-established correlations. The individual density (ρ_i) of each component and the compositional density of pellets packed in the bioreactor tray were determined using the following equations [14,23,24]:

$$\rho_w = 997.18 + 0.0031439\ T - 0.0037574\ T^2 \quad (1)$$

$$\rho_p = 1329.9 - 0.51814\ T \quad (2)$$

$$\rho_f = 925.59 - 0.41757\ T \quad (3)$$

$$\rho_c = 1599.1 - 0.31046\ T \quad (4)$$

$$\rho_{fi} = 1311.5 - 0.36589\ T \quad (5)$$

$$\rho_a = 2423.8 - 0.28063\ T \quad (6)$$

where ρ_w, ρ_p, ρ_f, ρ_c, ρ_{fi}, and ρ_a are the individual densities for water (w), protein (p), fat (f), carbohydrate (c), fiber (fi), and ash (a), respectively, and T is the temperature, in °C. The density of solids was calculated using the following equation:

$$\rho_b = \frac{1}{\sum X_i/\rho_i} \quad (7)$$

where ρ_b is the density of solids, X_i is the mass fraction of each component, and ρ_i is the individual density of each component.

The procedure proposed by Choi et al. [25] was applied to determine the thermal conductivity of the solid culture-based media. This method calculates thermal conductivity (k) based on the conductivities (k_i) and the volumetric fractions of each component (X_{vi}):

$$k_b = \sum(k_i X_{vi}) \tag{8}$$

Conductivity values in W·(m·K)$^{-1}$ were calculated at the required temperature (T, in °C) using the following equations:

$$k_w = 0.57109 + 0.0017625\ T - 6.7306 \times 10^{-6}\ T^2 \tag{9}$$

$$k_p = 2.2196 + 0.0062489\ T + 1.0154 \times 10^{-4}\ T^2 \tag{10}$$

$$k_f = 0.1807 + 0.0027604\ T - 1.7749 \times 10^{-7}\ T^2 \tag{11}$$

$$k_c = 0.2014 + 0.0013874\ T - 4.3312 \times 10^{-6}\ T^2 \tag{12}$$

$$k_{fi} = 0.18331 + 0.0012497\ T - 63.1683 \times 10^{-6}\ T^2 \tag{13}$$

$$k_a = 0.3296 + 0.001401\ T - 2.9039 \times 10^{-6}\ T^2 \tag{14}$$

where k_w, k_p, k_f, k_c, and k_{fi} are the conductivities for water, protein, fat, carbohydrates, fiber, and ash, respectively. The volumetric fraction of each component was determined using the following equation:

$$X_{vi} = \frac{X_i \rho_b}{\rho_i} \tag{15}$$

The conductivity of the solid culture medium packed in the bioreactor tray was calculated using the value of the fraction occupied by the solid culture medium (X_{vb}) and the void fraction (X_{va}). The solid-based fraction was calculated with the following equation, considering that the mass fraction of the solid culture medium is equal to 1:

$$X_{vb} = \frac{X_b \rho_{ap}}{\rho_b} \tag{16}$$

where X_b is the mass fraction of the solid culture-based medium and ρ_{ap} and ρ_{bs} are the apparent and real densities, respectively. The void fraction (X_{va}) was calculated by using the following equation:

$$X_{va} = 1 - X_{vb} \tag{17}$$

Thus, using X_{va}, the apparent density of the packed tray can be determined as $\rho_{ap} = \rho_b(1 - X_{va})$, and the apparent conductivity of the packed tray (k_{ap}) was calculated with the following equation:

$$k_{ap} = k_a X_{va} + k_b X_{vb} \tag{18}$$

The heat capacity of the solid-based medium was determined as a function of its components [26,27] using the following equation:

$$Cp_b = 1.42mc + 1.549mp + 1.675mf + 0.837ma + 4.187mw \tag{19}$$

where mc, mp, mf, ma, and mw are the individual mass fractions of carbohydrates (c), proteins (p), fats (f), ash (a), and water (w), respectively. Table 2 shows the calculated values for the thermal conductivity of the solid culture-based medium.

Table 2. Physical and thermodynamic properties of solid packed in the bioreactor tray.

Property		Value
Apparent density, ρ_{ap}	kgm^{-3}	828.6
Solid density, ρ_b	kgm^{-3}	1381.2
Thermic conductivity, k_{ap}	$W(mK)^{-1}$	0.158
Heat capacity, Cp_b	$(J)\ (gK)^{-1}$	1.840

2.7. Bench-Scale Packed-Tray Bioreactor

The concept of a wall-cooled packed-tray bioreactor emerged from the integration of the low-packing-height characteristic of tray bioreactors with the wall-cooled system and forced-aeration features of packed-column bioreactors. This design combines the benefits of both types, enhancing hydrodynamics and heat and mass transfer mechanisms essential for hosting SSF-valorizing AFBP-based substrates. The rectangular aspects of the tray were maintained to achieve a lower packing height; the challenge was designing the air diffuser to feed air (oxygen) by convection through the length packed with AFBP-based pellets and improve convective mass and heat transfer in the bioreaction zone.

Experimentation was carried out in this bench-scale packed-bed bioreactor to mimic the performance of *Yl*2.2ab under industrial scenarios. These scenarios include determining how fluid dynamics and mass transport impact the transport of oxygen to the solid-based phase inoculated with *Yl*2.2ab and how fluid dynamics and heat transport resistances, due to the poor conductivity of the solid-based medium (based on AFBP), affect the growth and metabolic activity of *Yl*2.2ab.

Figure 1 shows the bioreactor design, which, as mentioned earlier, was constructed as a rectangular vessel with a total volume of 4.5 L. It consists of two modules coupled together by stainless steel screws, and the top cover is integrated in the same way. The bioreactor was designed to include various sensors (instrumentation) to monitor in-line temperature, pressure drop, and species such as water, oxygen, and carbon dioxide [14].

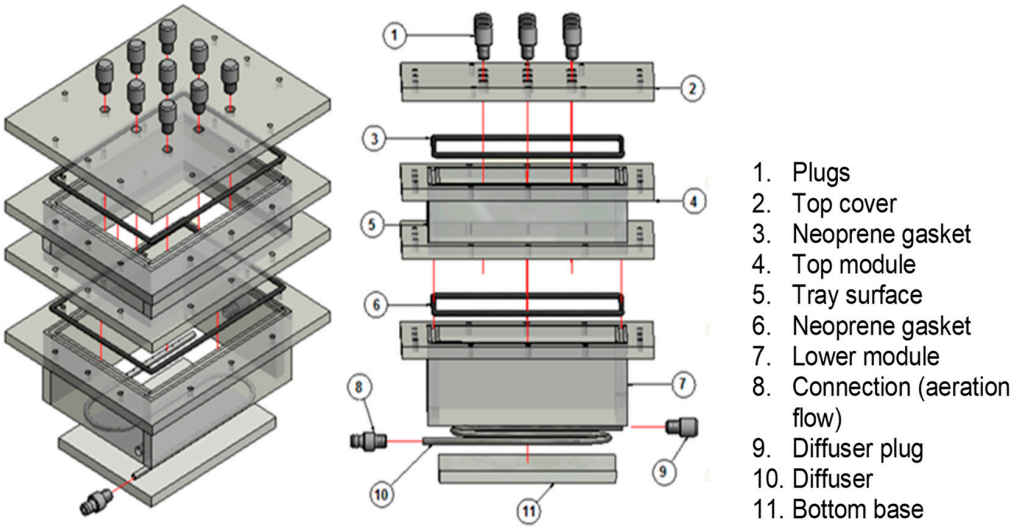

Figure 1. Body scheme and elements of the bench-scale packed-tray bioreactor.

Thus, the hypothesis behind the bioreactor design posited that the air diffuser would improve oxygen distribution along the packing length. Additionally, we hypothesized that the short packing length, convection, and cooling from the walls would regulate the temperature to levels favorable for *Yl*2.2ab growth and metabolic reactions based on laboratory results. Our third hypothesis was that this design would also reduce the drying of the solid-based medium. To assess these hypotheses, three different types of experiments were considered in the designed bioreactor:

(i) An abiotic heat transfer experiment was carried out to determine if the temperature could be homogeneous before starting the bioreaction at inlet volumetric flow rates of air of interest for SSF. It was essential to ensure that the temperature was conducive to optimal *Yl*2.2ab growth and protease production, as identified at the laboratory scale.
(ii) An abiotic mass transfer experiment was conducted to assess how oxygen is properly transported along the packing length at different volumetric flow rates.
(iii) A biotic experiment was carried out to elucidate how *Yl*2.2ab behaves under scenarios where fluid dynamics, mass transport, and heat transport mechanisms impact its growth and the production of proteases.

It is worth mentioning that these experiments, although preliminary, were essential for future experimental work associated with SSF-valorizing AFBP using *Yl*2.2ab. Table 3 shows the operating conditions and bed properties used during the abiotic experiments. Note that under the biotic experiment, the inlet flow rate of the air was 200 mL min^{-1}. Aside from this, the other operating conditions and bioreactor parameters were similar to the abiotic experiments.

Table 3. Bioreactor operating conditions in the abiotic studies.

Parameter	Magnitude
Fermentable solid mass	53.3% soybean paste and 43.7% fruit and vegetable by-products
Heating (cooling) system temperature	45 °C
Inlet flow rate (saturated air)	200, 300, and 400 mL min^{-1}
Packed-tray height	2 cm
Packed-try density	0.66 g cm^{-3}
Packed-tray mass (moistened)	400 g
Initial moisture of the bed	60%
Particle size of packing	1.41–1.68 mm
Void fraction of the packed bed	0.4

2.7.1. Airtightness Test

The bioreactor's airtightness was determined by testing two different types of neoprene O-ring gaskets, i.e., rectangular and round, as follows: first, aeration flow was supplied to the bioreactor. Then, the aeration flow was stopped, and the inlet and outlet valves were closed. Afterward, the pressure inside the system was recorded every 10 min for 1 h. This test was carried out before starting every experiment to ensure that the system was not leaking. Table 4 presents the properties of the gaskets, elucidating how the round gasket has a larger density than the rectangular one.

Table 4. Physical properties of neoprene O-ring gaskets.

	Neoprene Gaskets	
Geometry	**Rectangular**	**Circular**
Operating temperature	−40 to 93 °C	−20 to105 °C
Density	0.9 g cm^{-3}	1.45 g cm^{-3}
Thickness	6.35 mm	4.7 mm

Figure 2 displays the bioreactor system during the airtightness test, evaluating the round and rectangular gaskets. The rectangular gasket did not provide a hermetic seal, causing significant pressure drops. In contrast, the round gasket offered a tight seal of the system with no observed pressure drops. This was attributed to the larger density of the round gasket, leading to less deformation and a more robust seal between the modules that comprise the bioreactor body. Thus, during abiotic and biotic experiments, the round gasket was used to ensure a proper seal of the bioreactor.

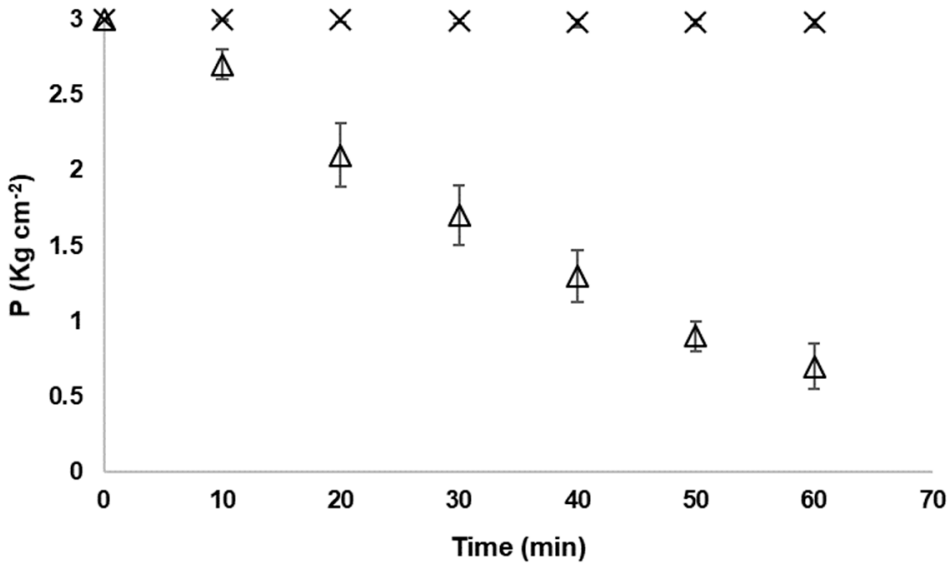

Figure 2. Comparison of the performance of bioreactor pressure under hermetic conditions when using round (X) and rectangular (Δ) O-ring gaskets.

2.7.2. Monitoring of Temperature

The temperature was measured in the packed tray using several thermocouples positioned in different zones. The temperature data were recorded online every 5 min using a data acquisition interface. During abiotic and biotic experiments, temperature was monitored at different positions of the packed region. Figure 3 shows the zones where the temperature was monitored to quantify temperature gradients from the inlet to the outlet and from the cooling system to the center of the packed region.

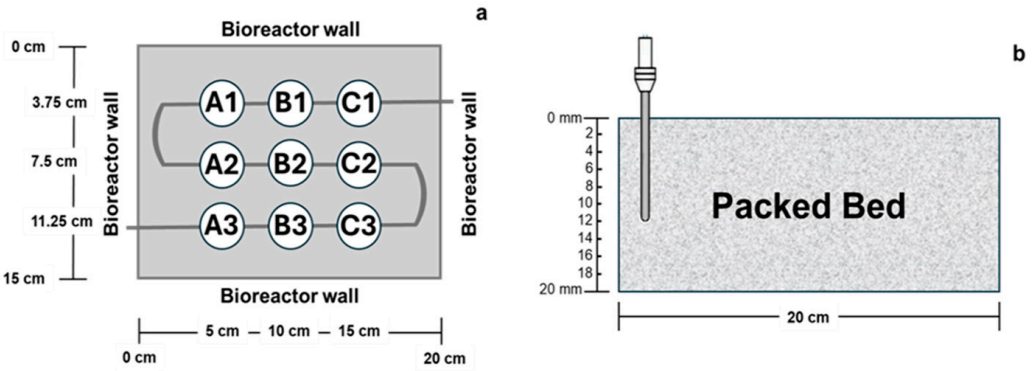

Figure 3. Zones where temperature was monitored to quantify temperature gradients from the inlet to the outlet and from the cooling system to the center of the packed region. (**a**) Positions where thermocouples were located during experiments, and (**b**) Lateral view of the packed tray (also referred to as the packed bed).

2.7.3. Respirometry

The macroscopic performance of *Yl*2.2ab was tracked by monitoring the consumption of O_2 and the production of CO_2 by the microorganism. The bioreactor was supplied with saturated air to ensure the microorganism's respiration (O_2) and remove the CO_2 and metabolic heat. The air effluent was dehydrated using a silica gel column. The air effluent was then directed to the gas chamber, where Vernier® CO_2/O_2 gas sensors measured the CO_2 and O_2 concentrations. The LabPro® interface and LoggerPro® software (https://www.vernier.com/downloads/logger-pro-demo/, accessed on 22 March 2024) of the Vernier® sensors performed the online data acquisition. Concentrations of CO_2 and O_2 were obtained as percentage values (mL gas per 100 mL of air).

2.8. Modeling and Simulations

The modeling of the packed-tray bioreactor was conducted using a hybrid framework. Before and after the bioreaction zone, Computational Fluid Dynamics (CFD)-based simulations were implemented to describe transport phenomena at the local level considering the system in 2 dimensions (2D). To model the packed tray (also referred to as the packed bed). When the microorganism was inoculated over the APBP-based pellets, biological reactions following a macroscopic approach were considered. The specifics of the two types of modeling, i.e., CFD and PCSs, can be reviewed in the literature [28,29]. Before and after the packed tray, the following governing equations ex-pressed in vectorial form were applied to simulate the performance of the bioreactor using CFD:

Hydrodynamics, considering that the fluid is incompressible and Newtonian, with values of μ_f and ρ_f associated with air supplied in the bioreactor:

$$\nabla \cdot \mathbf{u_f} = 0 \tag{20}$$

$$\rho_f \frac{\partial \mathbf{u_f}}{\partial t} = -\nabla p + \mu_f \nabla^2 \mathbf{u_f} \tag{21}$$

Mass transfer, considering the molecular diffusion of different species (CO_2, O_2, and H_2O) in nitrogen under diluted conditions. Fick's constitutive equation was used to describe diffusion mechanisms:

$$\frac{\partial c_{i_f}}{\partial t} = -\mathbf{u_f} \cdot \nabla c_{i_f} + \nabla \cdot \left(D_{i_f} \nabla c_{i_f} \right) \tag{22}$$

Heat transfer, considering Fourier's constitutive equation and the conductivity of air:

$$\rho_f C_{pf} \frac{\partial T_f}{\partial t} = -\rho_f C_{pf} \mathbf{u_f} \cdot \nabla T_f + \nabla \cdot \left(k_f \nabla T_f \right) \tag{23}$$

Initial and boundary conditions were assigned according to the physics associated with the bioreactor operation, which also depended on the operational conditions set for each experiment, under biotic or abiotic conditions.

The following heat and mass transfer governing equations based on PCSs using a 2D pseudo-homogeneous model, were used to describe transport phenomena and bioreactions in the packed zone, in which the AFBP-based support was inoculated with *Yl*2.2ab.

$$\frac{\partial c_{i_p}}{\partial t} = -\mathbf{u_p} \cdot \nabla c_{i_p} + \nabla \cdot \left(D_{i_p} \nabla c_{ip} \right) \pm \boldsymbol{\rho_{ap}} Y_{i/CO_2} R_{CO_2} \tag{24}$$

$$\rho_{pb} C_{pb} \frac{\partial T_p}{\partial t} = -\rho_f C_{pf} \boldsymbol{u_p} \cdot \nabla T_p + \nabla \cdot \left(k_{eff} \nabla T_p \right) + \underbrace{q_{evap}}_{evaporation} \quad \underbrace{+\boldsymbol{\rho_{ap}} (-\Delta H_{rc}) Y_{c/CO_2} R_{CO_2}}_{reaction} \tag{25}$$

Hydrodynamics was simulated using the model developed for the studied reaction system in our previous contribution [15]. It is worth noting that when the packing (AFBP-based pellets) in the tray was not inoculated with *Yl*2.2ab, reaction terms were not included in the heat and mass transfer governing equations. The initial and boundary conditions were as stated in the literature for the same reactor conception, i.e., the wall-cooled packed-bed reactor, and are given as follows considering a 2D pseudo-homogenous model [26–30]:

Initial conditions:

$$t = 0 \quad u_z = u_{zss} \tag{26}$$

$$C_{ip} = C_{i0} \tag{27}$$

$$T_p = T_{p0} \tag{28}$$

Boundary conditions:

$$z = 0 \quad u_{pz} = u_{z0} \tag{29}$$

$$u_{z0}c_{i0} = c_{ip}u_{pz} - D_{ip}\frac{\partial c_{ip}}{\partial z} \quad (30)$$

$$u_{z0}\rho_f Cp_f T_0 = u_{pz}\rho_f Cp_f T_p - k_{eff}\frac{\partial T_p}{\partial z} \quad (31)$$

$$z = L \quad \frac{\partial u_{pz}}{\partial z} = \frac{\partial c_{ip}}{\partial z} = \frac{\partial T_p}{\partial z} = 0 \quad (32)$$

$$x = 0x = R_{Wall}\frac{\partial u_{pz}}{\partial x} = \frac{\partial c_{ip}}{\partial x} = \frac{\partial T_p}{\partial x} = 0 \quad (33)$$

$$u_{pz} = 0 \text{ and } \frac{\partial c_{ip}}{\partial x} = \frac{\partial T_p}{\partial x} = 0 \quad (34)$$

$$-k_{\text{eff}}\frac{\partial T_p}{\partial x} = h_w(T_p - T_c) \text{ or } \frac{\partial T_p}{\partial x} = 0 \quad (35)$$

Although it is a simplified model to describe such a complex SSF process in a bench-scale bioreactor, it captures the main mechanisms involved in the catalytic bed, such as mass and heat transfer, convection, dispersion, conduction, evaporation, as well as the impact of the reaction. Hence, the 2D pseudo-homogeneous model worked for the present research, but it needs to be improved in future research for larger-scale applications. Complementing the experimental design behind the research hypotheses associated with the bioreactor design, the aim of the modeling was to conduct a preliminary study to shed light on the following:

(i) Determine how the forced-aeration dispersion system works, evaluating if its design properly impacts hydrodynamics, and how air is distributed along the packed tray.
(ii) Assess how oxygen is distributed in the packed tray since its presence is essential for different biological reactions.
(iii) Provide insights into the complex performance of the SSF and elucidate challenges in describing the performance of *Yl*2.2ab when using AFBP as a substrate source.

Numerical solutions of the governing equations describing the performance of the wall-cooled packed-tray bioreactor were carried out using the numerical framework of COMSOL Multiphysics 4.4®. To discretize and solve the parabolic partial differential equation, the finite element method (FEM) was used for the discretization of spatial terms, while the Backward Differentiation Formula (BDF) was used as the default time-stepping algorithm.

2.8.1. Bioreaction: Kinetics and Heat of Reaction

The global bioreaction based on empirical formulas for the studied system is presented in Equation (36) [26]. Table 5 presents yield coefficients obtained from elemental balances (C, H, O, and N) carried out for AFBP, *Yl*2.2ab, oxygen consumed, and $COCO_2$ and water produced from the metabolic activity of *Yl*2.2ab. In Equation (36), the stoichiometric balance is stated as a function of the production of CO_2, as can be identified from the yield coefficients.

$$Y_{S/CO_2}CH_{1.87}O_{0.71}N_{0.0913} + Y_{O_2/CO_2}O_2 \rightarrow Y_{X/CO_2}CH_{1.74}O_{0.45}N_{0.132} + CO_2 + Y_{W/CO_2}H_2O \quad (36)$$

Table 5. Yield coefficients associated with Equation (36).

Yield Coefficient	Value	Units
***Substrate*, Y_{S/CO_2}**	3.38	[mol S ·mol $CO_2{}^{-1}$]
***Oxygen*, Y_{O_2/CO_2}**	0.89	[mol O_2 ·mol $CO_2{}^{-1}$]
***Biomass*, Y_{X/CO_2}**	2.38	[mol X· mol $CO_2{}^{-1}$]
***Water*, Y_{W/CO_2}**	1.08	[mol W· mol $CO_2{}^{-1}$]

The macroscopic kinetic model coupled to the reactor model is given by the following equation:

$$R = R_{co_2} = \underbrace{\frac{dY_{co_2 p}}{dt} = \mu_x X_{co_2 p}\left(1 - \frac{X_{co_2 p}}{X_{co_2 max,}}\right)}_{Reaction\ rate} \tag{37}$$

$$R_i = \boldsymbol{Y_{i/CO_2}} R_{\boldsymbol{CO_2}}\ ;\ \ i:\ X, S, W,\ or\ C \tag{38}$$

This unstructured model is well-known in the literature as the logistic kinetic model [7], commonly used to analyze microbial growth kinetics from a macroscopic perspective. Kinetic parameters such as μ_x and $c_{co_2 max}$ were varied to elucidate their influence on the performance of the bioreactor design around the apparent ones.

The enthalpy of the bioreaction in Equation (25) must be calculated, using the carbon involved in species reacting and being formed during the biological reaction as the reference; its calculation is based on the following thermodynamic-based equation:

$$\Delta H_{rc} = \sum n_p \Delta H_{C_{Products}} - \sum n_r \Delta H_{C_{Reacteants}} \tag{39}$$

where $\Delta H_{C_{Products}}$ and $\Delta H_{C_{Reacteants}}$ are the combustion enthalpies of products and reactants associated with the carbon present in their structures, respectively, while n_i is the number of moles of species i. Note that the enthalpy of the reaction was calculated using stoichiometric coefficients based on biomass such that Equation (36) becomes Equation (40).

$$1.42\ CH_{1.87}O_{0.71}N_{0.0913} + 0.37\ O_2 \rightarrow\ CH_{1.74}O_{0.45}N_{0.132} + 0.42\ CO_2 + 0.45\ H_2O \tag{40}$$

To calculate combustion-based enthalpies, Tillman's correlation (Equation (41)) was applied to the substrate and biomass [31].

$$\Delta H_C = 188\ C - 718\ \frac{Btu}{lb} \tag{41}$$

where C is the percentage of carbon involved in the empirical formula stated in Equation (40), as follows:

$$\Delta H_C(Substatre - based\ source) = 9434\ \frac{Btu}{lb} = 582\ \frac{kJ}{mol} \tag{42}$$

$$\Delta H_C\ (Biomass) = 9095.6\ \frac{Btu}{lb} = 482.76\ \frac{\text{kJ}}{\text{mol}} \tag{43}$$

$$\Delta H_{rc} = 482.76\ \text{kJ}\ (\text{mol})^{-1} - 1.42\left(582\ \text{kJ}\ (\text{mol})^{-1}\right) = -343\ \text{kJ}\ (\text{mol})^{-1} \tag{44}$$

2.8.2. Model Parameters

Table 6 presents the model parameters used in the solution of the bioreactor model. Most parameters were determined from correlations, while others were calculated in this work.

Table 6. Model parameters used during simulations of the performance of the bioreactor design under abiotic and biotic conditions.

Parameter	Description	Units	Value	Status
k_f	Thermal conductivity of air	W $m^{-1}K^{-1}$	0.027	-
C_{pf}	Specific heat capacity of air	kJ kg^{-1} K^{-1}	1.005	-
μ_f	Dynamic viscosity of air	Pas	0.01907	-
ρ_f	Density of air	kgm^{-3}	1.13	-
ρ_b	Solid-based density	kgm^{-3}	1381.2	Calculated

Table 6. *Cont.*

Parameter	Description	Units	Value	Status
ρ_{ap}	Packed-tray density	kgm^{-3}	828.6	Calculated
Q_{in}	Inlet flow rate	cm^3min^{-1}	200–400	Operation variable
ϵ	Void fraction in the tray	*Dimensionless*	0.4	Calculated
d_p	Pellet diameter	mm	1.41–1.68	Calculated
D_{ip}	Effective dispersion coefficient	m^2s^{-1}	1.67×10^{-11}	Calculated
k_{eff}	Effective thermal conductivity	$W\ m^{-1}K^{-1}$	0.1048	[32]
k_{ap}	Thermal conductivity of the solid	$W\ m^{-1}K^{-1}$	0.158	Calculated
μ_{CO_2}	Apparent specific rate coefficient based on the production of CO_2	h^{-1}	0.64	Calculated
$X_{CO_{2max}}(c_{CO_{2max}}/\rho_{ssdb})$	Apparent coefficient of the maximum amount of CO_2	$m_{gCO2}\ g_{ssdb}{}^{-1}$	153.48	Calculated
h_w	Wall heat transfer coefficient	$W\ m^{-2}K^{-1}$	0.0511	[29]
	Bed height	m	0.02	Calculated
T_c	Coolant temperature	K	313	Operation variable
T_0	Inlet temperature in the packed tray	K	313	Operation variable
T_r	Inlet temperature in the system	K	298	Operation variable
M	Moisture content	%	60	Operation variable

3. Results and Discussion

This section is divided into three subsections to emphasize the main results of this contribution. Section 3.1 presents results associated with hydrodynamics, with the aim of assessing how the in-house air distributor works and analyzing the flow patterns before and after the packed zone as well as within it. Section 3.2 shows the results associated with mass transfer under abiotic conditions, providing inferences on how oxygen present in the fed air is transported and distributed in the bioreaction region. Section 3.3 analyzes heat transfer under abiotic conditions to evaluate how the cooling system works and to elucidate the magnitude of the temperature gradient in the bioreactor design, especially in the bioreaction region, which is packed with the AFBP-based substrate and has lower conductivity compared to synthetic-based supports. To this end, the experimental results are presented, followed by modeling results. Finally, Section 3.4 presents the experimental results of the performance of *Yl*2.2ab in the bench-scale bioreactor. Due to the heat released by the reaction and the low conductivity of the AFBP-based substrate, temperature gradients are expected. Thus, by analyzing macroscopic respirometry data, monitoring the in situ bed temperature, and measuring protease activity over time, Thus, by analyzing macroscopic respirometry data, monitoring the in situ bed temper-ature, and measuring protease activity over time, the extremophilic properties of *Yl*2.2ab, identified under laboratory-controlled conditions, are now being assessed in a bench-scale bioreactor. Additionally, the simulation results obtained with the hybrid-based model are pre-sented to evaluate how transport phenomena impact macroscopic kinetics. Additionally, the simulation results obtained with the hybrid-based model are presented to evaluate how transport phenomena impact macroscopic kinetics.

3.1. Hydrodynamics

Figure 4a–c displays the velocity field at steady state in the bench-scale bioreactor when the inlet flow rate was varied at three levels: 200 mL min^{-1}, 300 mL min^{-1}, and 400 mL min^{-1}. Figure 4d shows the streamlines in the bioreactor, elucidating how the fluid flow patterns were distributed throughout the different regions of the system. Figure 5 displays how the average velocity profile performs along the x-axis, where molecular momentum mechanisms are dominant. The bioreactor can be analyzed in three regions: the first region, i.e., the air distributor, where the in-house designed system feeds the air; the second region, i.e., the packed bed, where the biological reactions take place; and the third region, associated with the head of the reactor, where gases exit the reactor.

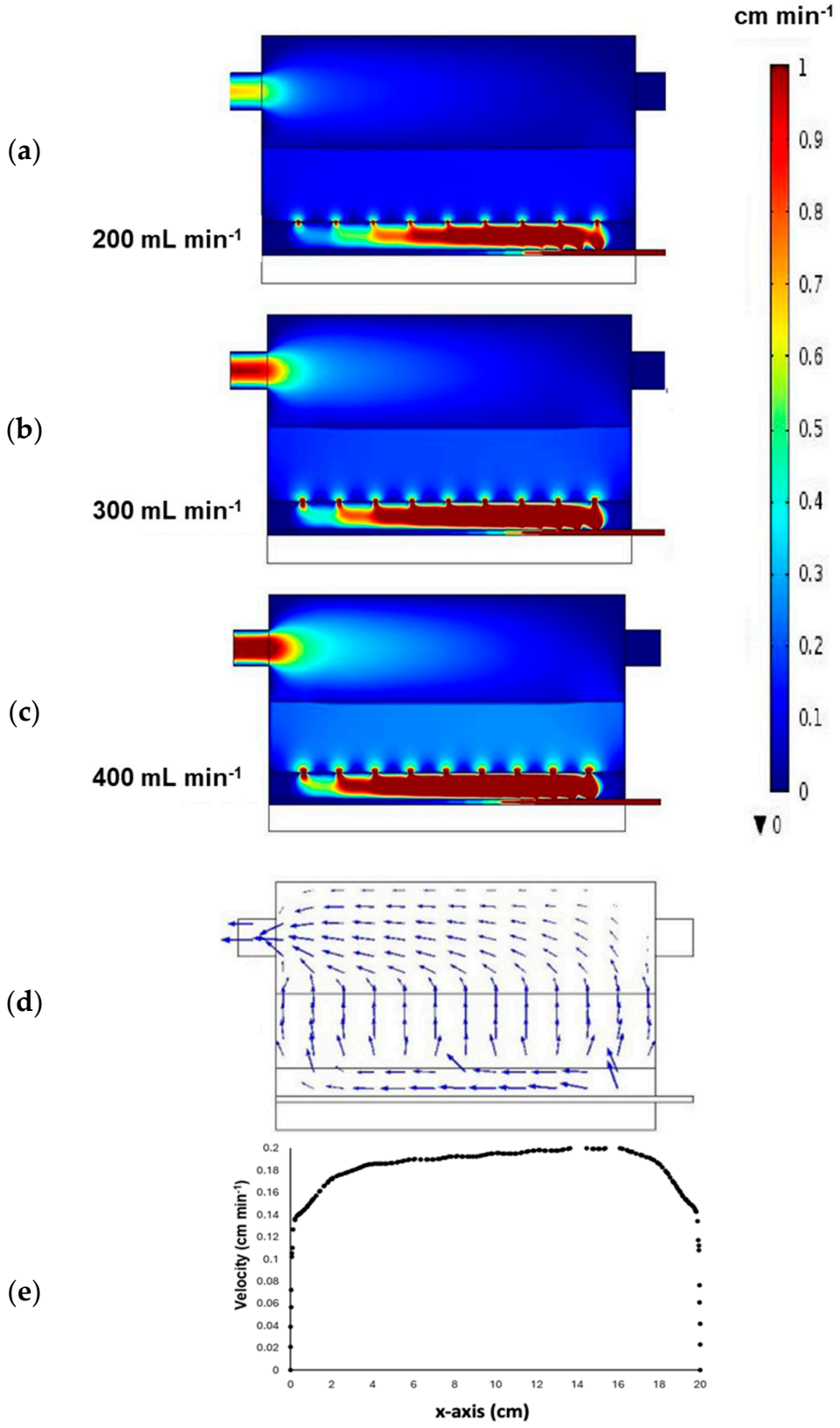

Figure 4. Hydrodynamics in the bench-scale bioreactor: (**a**–**c**) velocity fields predicted as a function of the inlet volumetric flow rate determined at normal conditions of pressure and temperature: 200, 300, and 400 mL min^{-1}; (**d**) streamlines simulated in the bench-scale bioreactor for an inlet flow rate of 300 mL min^{-1}; and (**e**) velocity profile along the x-axis for an inlet flow rate of 300 mL min^{-1}.

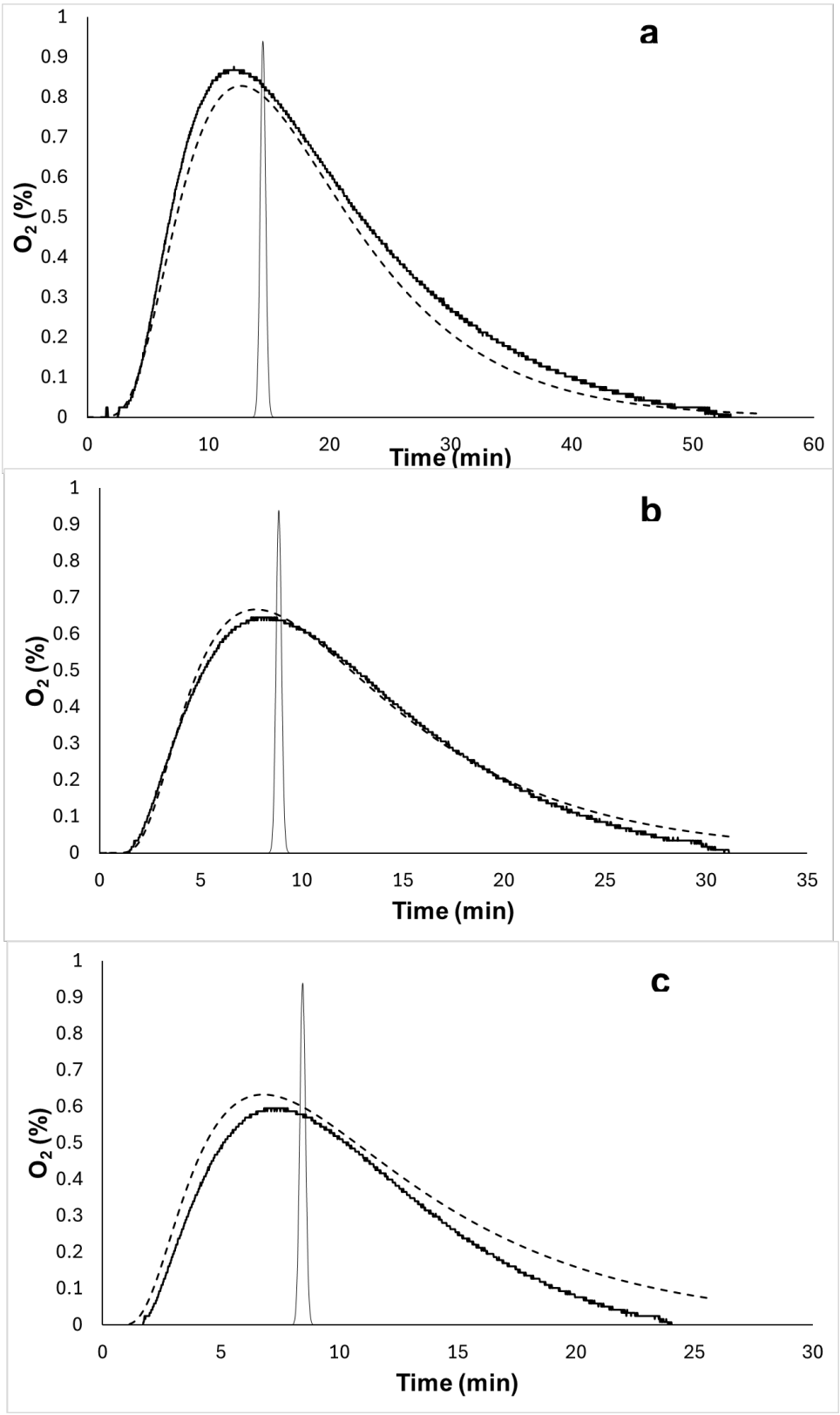

Figure 5. RTD curves obtained in the bench-scale bioreactor when varying the inlet volumetric flow rate: (**a**) 200 mL min^{-1}; (**b**) 300 mL min^{-1}; (**c**) 400 mL min^{-1}; (~~~~) Observed curve; (– – –) predicted curve; and (——) ideal curve.

Based on these hydrodynamic results, streamlines were obtained (Figure 4d), and the flow patterns corroborate what was elucidated from the velocity fields. When the average

velocity magnitude along the x-axis was plotted (Figure 4e), it was inferred that the main shear stresses over the fluid were at the wall, while a pseudo-hydrodynamic plug flow was observed at the core of the bed. Note that based on our hydrodynamic results for the bench-scale packed-tray bioreactor, published in 2019 [15], due to the tube-to-particle diameter ratio, the void fraction was considered constant in the packed region since most of the x-axis and z-axis lead to a pseudo-constant void fraction, while the main fluctuations in void fractions were associated with the wall zone. The inlet flow rate used to obtain Figure 4d,e was 300 mL min^{-1}, which was the flow rate applied during experimentation under biotic conditions, as discussed in Section 3.4.

The distributor worked in a promising way, feeding air through the whole packed region. This is essential for two aspects: moving metabolic heat once the biological reaction starts and feeding oxygen to *Yl*2.2ab for its metabolic-based oxidation reactions. Nevertheless, at this time, a warning must be given regarding the pressure drop, as identified in 2019 [15], since the accessories, including the air distributor and the outlet flow design, and pellet diameters used to pack the bioreaction region led to high pressure drops (the pressure drop increases from 0.1 to 30,000 Pa m^{-1}), which can have a negative impact on cost when scaling up the bioreactor.

3.2. Oxygen Mass Transport

3.2.1. Experimentation

To analyze how the mass transfer dispersion of oxygen impacts bioreactor performance, particularly in the packed region, residence time distribution (RTD) curves were first obtained experimentally for oxygen at different inlet flow rates: 200 mL min^{-1}, 300 mL min^{-1}, and 400 mL min^{-1}. Figure 5 displays RTD curves for oxygen under different scenarios at the mentioned inlet flow rates, comparing experimental observations, model predictions when determining the dispersion coefficient for oxygen, and the ideal RTD curve for oxygen when there is no dispersion phenomenon involved in the bioreactor. Taking the ideal RTD curve as a reference, it was identified that significant dispersion mechanisms are involved in the studied bioreactor at the inlet flow rates studied. Three regions in the bed can contribute to these dispersion mechanisms, making it difficult to elucidate the dispersion mechanisms for the packed region. Therefore, dispersion analysis was carried out following Levenspiel's approach [33], in which RTD curves were obtained by introducing a tracer pulse of oxygen at the inlet and measuring its concentration at the outlet over time. This method determined the dispersion coefficient for the entire reactor rather than just the packed region.

The procedure for the determination of the dispersion coefficient is described below:

(i) Tracer experiment: a known amount of oxygen-based tracer was injected into the bioreactor, and the outlet concentration was monitored as a function of time (see Figure 5).

(ii) Normalizing the RTD curve: oxygen concentration-based data were normalized to obtain the exit age distribution function:

$$E(t) = \frac{C_{O_2}(t)}{\int_0^\infty C_{O_2}(t)\,dt} = \frac{C_{O_2}(t_i)}{\sum C_{O_2}(t_i)\Delta t_i} \tag{45}$$

(iii) Calculating moments: the mean residence time and variance were computed:

$$\bar{t} = \int_0^\infty tE(t)dt = \frac{\sum t_i C_{O_2}(t_i)\Delta t_i}{\sum C_{O_2}(t_i)\Delta t_i} = \frac{\sum t_i C_{O_2}(t_i)}{\sum C_{O_2}(t_i)} \tag{46}$$

$$\sigma^2 = \int_0^\infty \left(t - \bar{t}\right)^2 E(t)dt \tag{47}$$

(iv) Determining the dispersion coefficient (D_i): the relationship between the variance and the dispersion coefficient was applied to calculate D_i:

$$\sigma^2 = \frac{2D_iL}{{u_o}^2} + \frac{L^2}{{u_o}^2} \quad (48)$$

$$D_i = {u_o}^2\left(\frac{\sigma^2 - \left\{\overline{t}\right\}^2}{2L}\right) \quad (49)$$

The dispersion coefficients were determined and then used to predict RTD curves, as presented in Figure 5. Observations were predicted properly considering experimental deviations. As the inlet flow rate increased, deviations were higher but acceptable, providing a clear idea of the effect of dispersion mechanisms in the transport of oxygen species in the bioreactor. Table 7 presents the values for the module $\frac{D_i}{u_oL}$ for each inlet flow rate, considering that u_o was taken as the inlet velocity calculated from the inlet flow rate and L is the length of the packed region. Note that D_i is an apparent parameter that contains dispersion mechanisms involved in the three regions of the bioreactor: distributor-based, packed, and head regions. To this end, these results suggest that diffusion, back-mixing, and even dead zones play significant roles in the overall dispersion observed in the bioreactor. The value of the module decreases as the inlet flow rate increases, indicating that at larger inlet flow rates, back-mixing mechanisms become dominant. As a reference. [34] reported that $\frac{D_i}{u_oL}$ = 0.141 for a tubular-based reactor, using bromocresol green as a tracer and a bed with a void fraction of 0.4, while Rojas et al. [35] reported that $\frac{D_i}{u_oL}$ = 0.145 for an industrial leaching system, adjusting the experimental values to the serial tank dispersion model.

Table 7. Parameters determined from RTD curves.

Flow (mL min^{-1})	**Experimental**		
	$\overline{t}$	σ^2	D_i/u_oL
200	18.78	89.15	0.125
300	11.89	33.75	0.117
400	10.52	19.92	0.102

3.2.2. Simulations

Once the dispersion coefficient was determined via RTD curves, this parameter, although apparent, was used to predict oxygen concentration profiles in the bioreactor, considering it isothermal at 40 °C. Figure 6a depicts the bioreactor's oxygen concentration via a surface predicted at three different operational times (0, 1, and 6 h) and different inlet flow rates (200 mL min^{-1}; 300 mL min^{-1}; and 400 mL min^{-1}). Figure 6b shows the average oxygen concentration obtained from the surface prediction in the packed region of the bioreactor as a function of time at the three inlet flow rates. Note that in these simulations, hydrodynamics was coupled to the mass transport equation under abiotic conditions. At any inlet flow rate, oxygen reached all zones within the packed region at the desired concentration, demonstrating that the oxygen distributor design worked as expected. Regarding the time for the oxygen concentration to reach a pseudo-steady state in the packed region, it took 2 h for the lowest inlet flow rate, while it took 4 h at the highest inlet flow rate due to the effect of the residence time, which is lower for the highest inlet flow rate. Although these simulations were obtained under abiotic conditions, as hypothesized, oxygen would be present before 4 h in the packed region at the studied inlet flow rates. This suggests that once the biological reactions initiate, there would be sufficient oxygen for their metabolic activity, appropriately accomplishing one of the challenges during SSF.

(**a**)

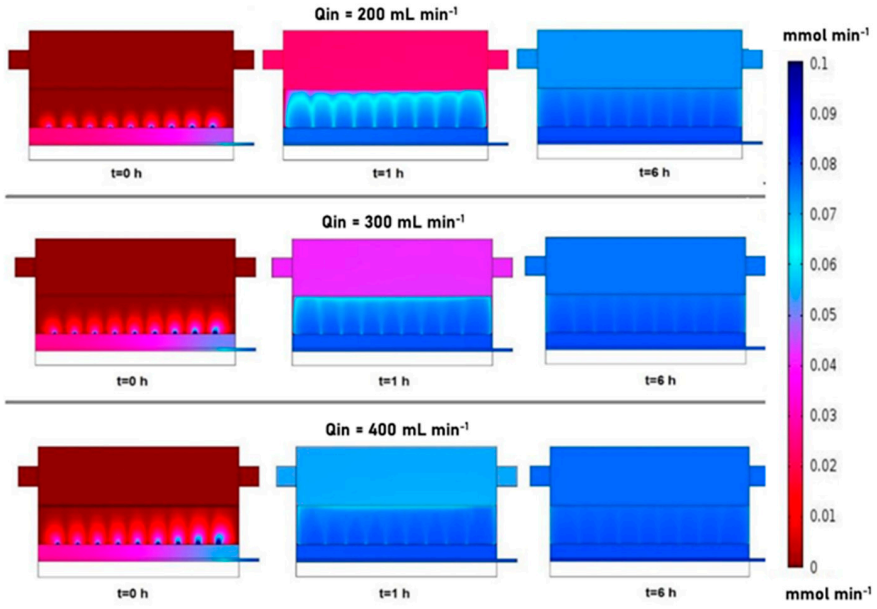

(**b**)

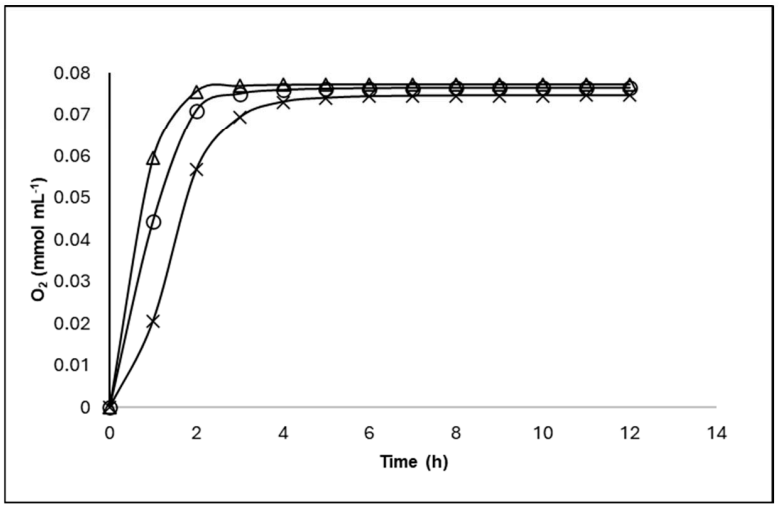

Figure 6. Oxygen mass transport in the bioreactor: (**a**) Concentration predicted surface obtained at different operational times and different inlet flow rates; and (**b**) average concentration profile obtained from the concentration predicted surface: (x) 200 mL^{-1}; (○) 300 mL^{-1}; (Δ) 400 mL^{-1}.

3.3. Heat Transfer

3.3.1. Experimentation

Considering that one of the challenges of using AFBP-based substrate during SSF is designing a reactor that can overcome its low thermal conductivity, the following discussion presents heat transfer under abiotic conditions to elucidate whether conductive and convective heat transfer mechanisms can homogenize the temperature in the packed region before the bioreaction initiates. Figure 7 displays the temperature profiles along the z-axis at different inlet flow rates: 200 mL min^{-1}, 300 mL min^{-1}, and 400 mL min^{-1}. Considering that temperature monitoring was carried out at the center of the bed, a packed-bed depth of 0 mm is located at the exit of the packed region (z = 20 mm), and a packed-bed depth of 20 mm is located at the start of the bed (z = 0 mm), while the coolant temperature was fixed at 45 °C and the inlet temperature of the bioreactor was fixed at 20 °C, the following can be identified:

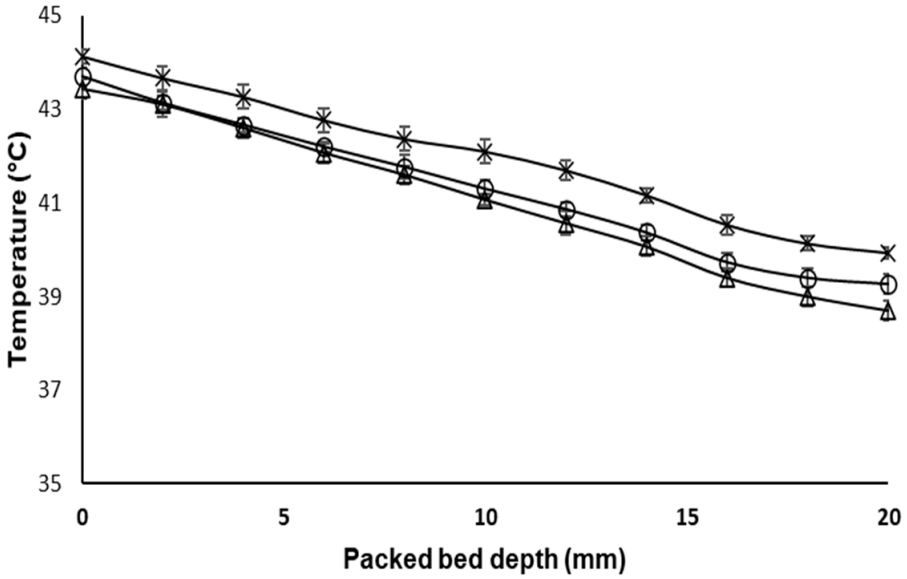

Figure 7. Temperature profile along the depth of the packed bed (x-axis) at different inlet flow rates: (x) 200 mL min^{-1}, (○) 300 mL min^{-1}, and (Δ) 400 mL min^{-1}.

The temperature gradient along the z-axis of the packed bed varies with the inlet flow rate. As the inlet volumetric flow increased, cooling by convection also increased such that at z = 0 mm, the inlet temperature in the packed region was 39 °C at 400 mL min^{-1}, while it was 41 °C at 200 mL/min. Considering that the whole bioreactor was submerged in a water-based coolant system with a temperature of 45 °C, it is clear that the residence time in the distributor zone was insufficient to heat the fluid to the desired temperature of 45 °C. In fact, the fluid being transported through the packed region at any inlet flow rate did not reach the coolant temperature, elucidating heat transfer resistances by conduction along the x and y axes, with temperature gradients ranging from 2 to 6 °C at an inlet volumetric flow rate of 400 mL min^{-1} and from 1 to 4 °C at an inlet volumetric flow rate of 200 mL min^{-1}.

Due to the residence time of fluid in the bioreactor, at higher inlet flow rates, the temperature reaches higher values, approaching the coolant temperature. Since at time zero, the entire packed region was at 45 °C, it can be inferred that, on the one hand, the air being supplied to the reactor must be fed at temperatures closer to the coolant temperature since convective heat transfer is dominant in the bed. To this end, feeding the fluid at larger inlet temperatures in the distributor zone will help achieve the desired metabolic temperature in the packed zone once biological reactions begin. On the other hand, once the reaction initiates in the packed region, the low conduction of the AFBP-based substrate will cause metabolic heat to accumulate in the bioreactor, making convection rather than radial cooling the main mechanism for cooling the bioreaction zone. This suggests that the reactor design must be improved to enhance heat transfer mechanisms.

As a reference, Ashley et al. [36] reported a 5 °C difference between the outlet (40 °C) and inlet (35 °C) temperatures when feeding air in a tubular bioreactor in the absence of microbial growth. During fermentation, temperature gradients caused increments in temperature in the packed-bed bioreactor, with lower temperatures at the bioreactor inlet. The lower part of the bed presented lower temperatures due to the convective mechanism and the lower temperature of the fed air, while at higher parts of the bed, convection was insufficient to remove metabolic heat.

3.3.2. Simulations

To carry out heat transfer simulations, essential parameters such as effective thermal conductivity (k_{eff}) and wall heat transfer coefficient (h_w) are necessary to accurately describe temperatures in the packed region. These parameters were determined from correlations and need to be properly verified in future studies for the system under investigation. The

aim of the heat transfer simulations in this section was to demonstrate how convective and conductive mechanisms interact to cool the bioreactor.

Figure 8 displays temperature surface plots obtained at different times (0–8 h) for the bioreactor when operated under various inlet flow rates (200–400 mL min^{-1}). The aeration flow temperature in the bioreactor inlet was maintained at 20 °C, while it is assumed that the initial temperature for starting up the experiments was 45 °C throughout the bioreactor. Once the air is fed, the bioreactor operates in adiabatic mode. As the inlet volumetric flow rate increases, convective heat transfer becomes more effective in removing heat from the bioreactor. Nevertheless, due to the low conductivity of the AFBY-based packing, cooling the bioreactor from 45 to 20 °C requires more than 8 h at inlet flow rates of 200 mL min^{-1} and 300 mL min^{-1}, while it takes 8 h at 400 mL min^{-1}. Although preliminary, these abiotic simulations suggest that convective heat transfer alone might not be sufficient to cool the bioreactor, agreeing with the literature when using AFBY as a substrate-based source during SSF [36].

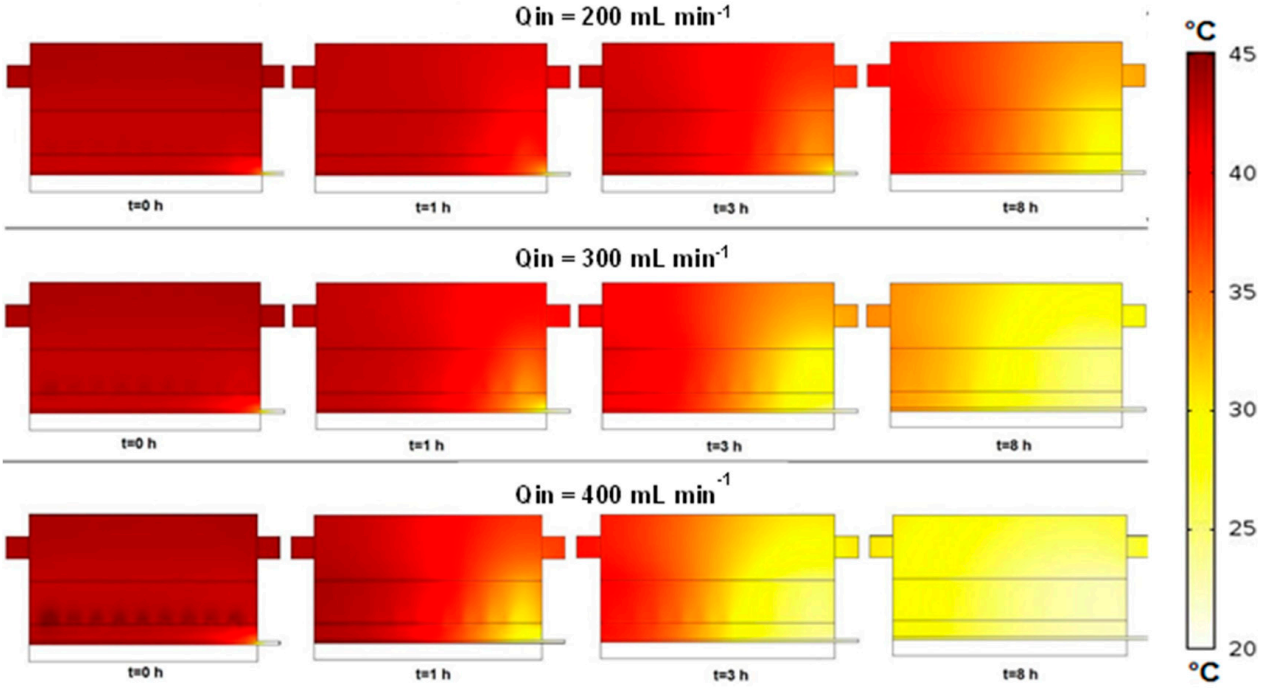

Figure 8. Temperature surface plots were obtained in the bioreactor at different inlet flow rates of 200 mL min^{-1}, 300 mL min^{-1}, and 400 mL min^{-1}. The inlet temperature was set to 20 °C, and the initial temperature was 45 °C, with the bioreactor operating in adiabatic mode.

3.4. Solid-State Fermentation

3.4.1. Experimentation

Figure 9 displays transient profiles associated with the production rate of carbon dioxide, the consumption rate of oxygen, the temperature at the outlet of the packed region, and the proteolytic activity of *Yl*2.2ab. These transient profiles were obtained in the bench-scale bioreactor, which operated with an inlet volumetric flow rate of 300 mL min^{-1} of saturated air, an inlet temperature of 20 °C, an initial moisture content of 60% in the solid mass, and a coolant temperature of 45 °C. Based on the observed CO_2 production rate, *Yl*2.2ab experienced an adaptation period (lag phase) of approximately 8 h. Following this phase, the microorganisms began to actively metabolize the substrate, entering an exponential growth phase that spanned from 8 to 12 h, with a peak production rate occurring at 12 h. After this peak, there was a significant and constant decline in CO_2 production between 12 and 20 h. Following this decline, the CO_2 production rate exhibited a more gradual decrease, observed from 20 to 40 h.

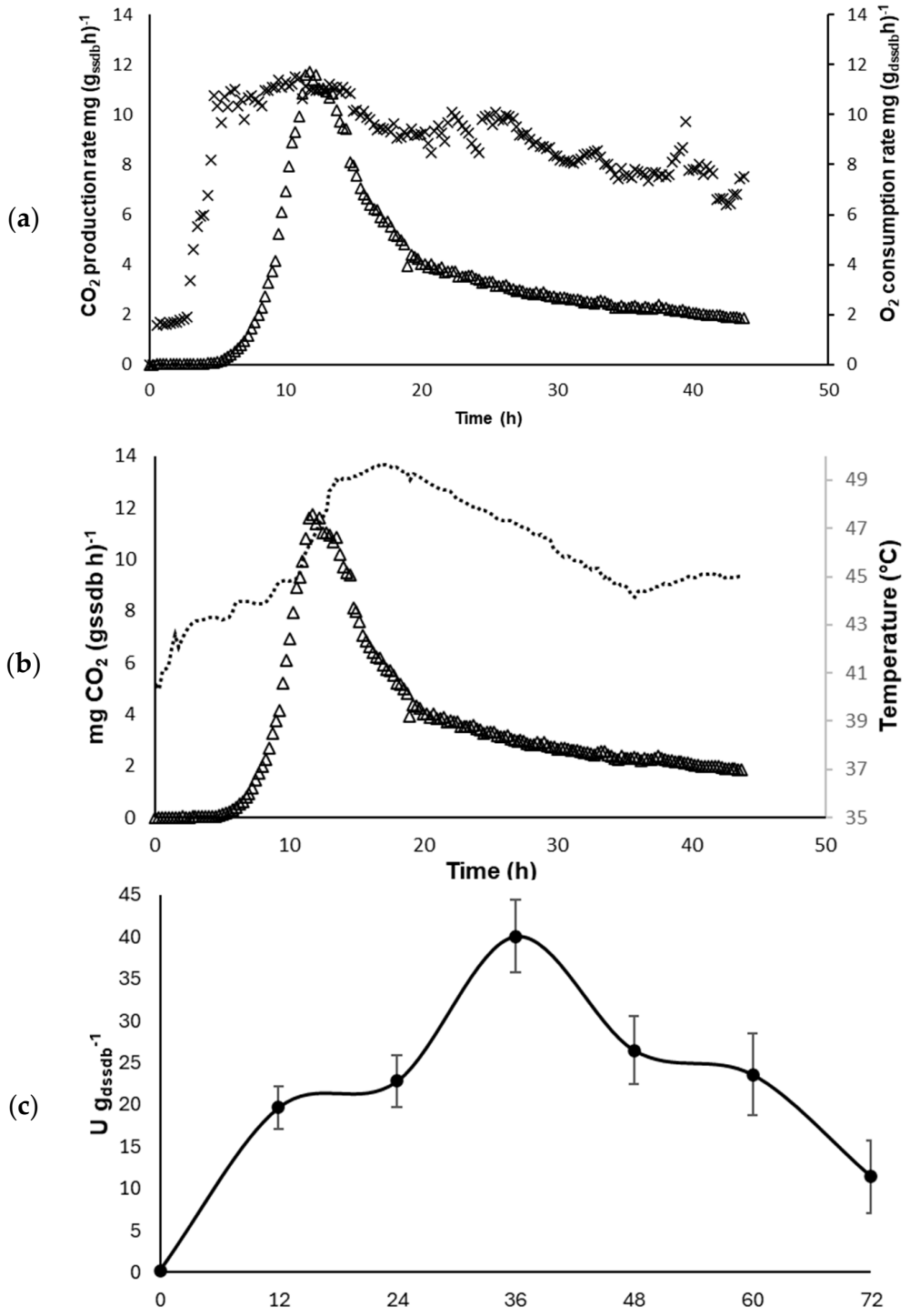

Figure 9. Biotic experiments were conducted in the bench-scale packed-tray bioreactor. An inlet volumetric flow rate of 300 mL min^{-1} with saturated air, an inlet temperature of 20 °C, an initial moisture content of 60% in the solid mass, and a coolant temperature of 45 °C were applied. (**a**) The production rate of CO_2 and the consumption rate of O_2. (**b**) The CO_2 production rate and temperature monitored at the center of the top surface of the packed region. (**c**) Protease production by *Yl* 2.2ab in the bench-scale packed-tray bioreactor. (Δ) CO_2 production rate; (x) O_2 consumption rate; and (. . .) temperature.

When relating the CO_2 production rate to the oxygen consumption rate (Figure 9a), temperature (Figure 9b), and proteolytic activity (Figure 9c), the following three aspects can be inferred:

(i) Oxygen was consumed throughout the entire experiment by *Yl*2.2ab, with higher consumption observed in the range of 6 to 16 h (from 10 to 12 mg $g_{ssdb}{}^{-1}$ h^{-1}). The minimum consumption rate was observed before 6 h (from 2 to 10 mg $g_{ssdb}{}^{-1}$ h^{-1}). It is worth noting that appreciable consumption of oxygen was identified from 16 to 45 h (from 6 to 10 mg $g_{ssdb}{}^{-1}$ h^{-1}), even when the microorganisms had already entered the stationary phase. This trend in oxygen consumption during the biological process can be explained by the distinct phases of microbial growth and metabolism. Initially, in the lag phase, microorganisms adapt to their new environment, resulting in low oxygen consumption. As they transition to the exponential growth phase, their metabolic activity surges, leading to a significant increase in oxygen consumption. During the subsequent phase, as the microorganisms approach the stationary phase, nutrient decrement, associated with mass transport resistances or depletion, and product accumulation slow their growth or production rate of $COCO_2$. Despite this, oxygen consumption remains considerable because the microorganisms continue to need oxygen for essential maintenance and cellular functions.

(ii) Regarding temperature, when the flow of air was supplied, the temperature decreased to 41 °C at the outlet of the packed region due to convective cooling, as demonstrated in our abiotic heat transfer experiment. However, during the lag and exponential phases, the metabolic activity of the microorganisms increased, causing the temperature to rise to 49 °C, with the peak recorded at 18 h. This rise in temperature is due to the exothermic nature of microbial metabolism, along with the low thermal conductivity of the substrate-based packing or significant heat transfer resistances in the core and wall of the packed region. Once the microorganisms entered the stationary phase and the $COCO_2$ production rates decreased significantly, the metabolic heat generation diminished, causing the temperature to decrease to 45 °C at 36 h, where it then stabilized.

(iii) Concerning proteolytic activity, it reached a maximum at 36 h of fermentation. This peak occurred when the temperature was close to the optimal level of 45 °C, as determined in laboratory-scale controlled conditions [2]. At this point in the fermentation, *Yl*2.2ab had entered the stationary phase, characterized by a low production rate of $COCO_2$ and a significant consumption rate of OCO_2. The optimal temperature likely enhanced enzyme activity, contributing to the observed peak in proteolytic activity. Consequently, after 36 h, as the metabolic processes stabilized and nutrient availability decreased, the proteolytic activity subsequently declined.

As a reference, most yeasts have an exponential growth time ranging from 1 to 2 h, corresponding to an apparent growth rate of 0.7 to 0.35 h^{-1} [37,38]. The apparent rate of CO_2 production obtained in this study was 0.53 h^{-1}. The maximum $COCO_2$ production rate obtained in this study was approximately 12 mg $g_{ssdb}{}^{-1}$ h^{-1}, which is much higher than the value reported for M. anisopliae (0.37 mg $g_{ssdb}{}^{-1}$ h^{-1}) [37,38].

3.4.2. Simulations

Figure 10 displays a sensitivity study of bioreactor performance, varying the maximum specific growth rate (μ_X). Simulations were carried out with the model and parameters presented in Section 2.8 under biotic conditions. Given that many transport phenomena and macroscopic parameters are unknown for the studied bioreactor, transport parameters were obtained from the literature, and macroscopic kinetic parameters were varied around an initial value determined using conventional methodologies that neglect transport phenomena, relying solely on Equation (37).

(**a**)

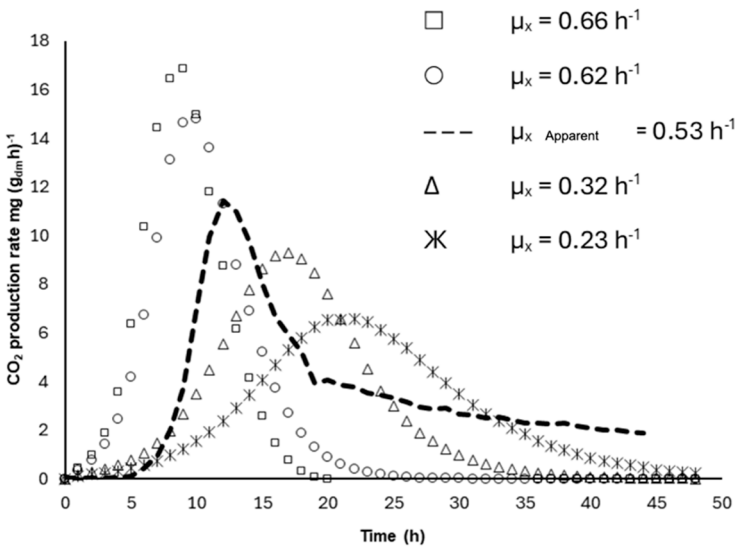

(**b**)

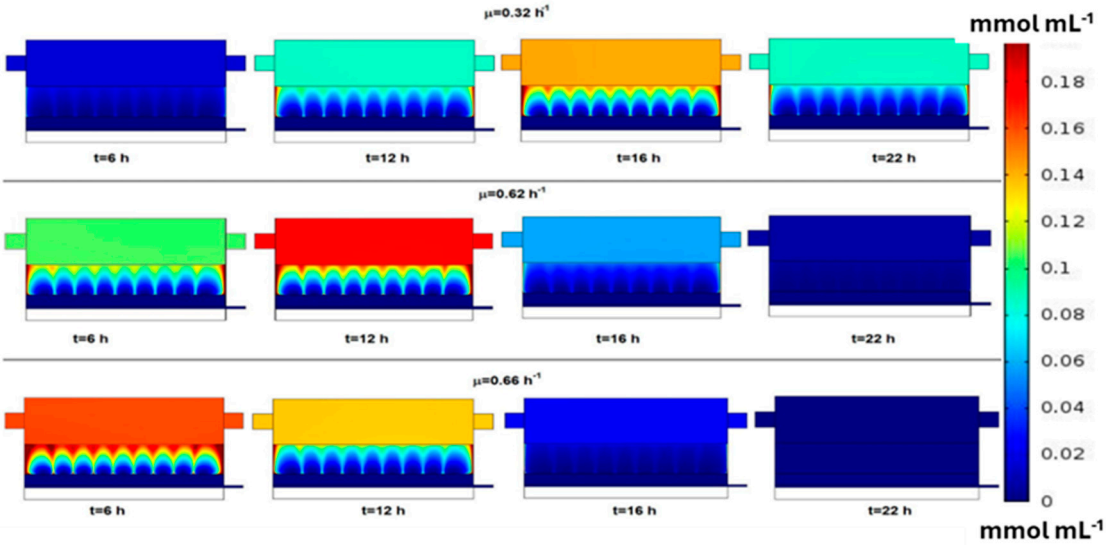

Figure 10. Production of CO_2 using different values of the specific growth rate (μ_X) for *Yl2.2ab*. (**a**) Model predictions of the production rate of CO_2 throughout the fermentation. (**b**) Surface plots showing the concentration of CO_2 in the reactor at different times.

Figure 10a shows our bioreactor simulations when μ_X was varied from 0.23 to 0.66 h^{-1}, finding that μ_X = 0.53 h^{-1} is a parameter that closely describes observations related to the production rate of CO_2 (see Figure 9). These simulations elucidate the complex interaction of transport phenomena and kinetics, demonstrating that small variations in μ_X lead to different performance outcomes. Given the uncertainty in characterizing transport phenomena, this parameter for *Yl*2.2ab can be considered an apparent one. It indicates that it only works for our microorganism and can be influenced by other mechanisms that were not properly characterized, such as convective and dispersive heat and mass transport mechanisms, including fluid dynamics.

Figure 10b presents surface plots of the concentration of CO_2 in the bioreactor. In these simulations, three cases were considered: μ_X (or μ) = 0.32, 0.62, and 0.66 h^{-1}. As illustrated in Figure 10a, the value of μ significantly impacted the phases involved in microorganism growth, such that a higher value accelerates all phases, resulting in higher concentrations of CO_2 at earlier times, and vice versa. These simulations demonstrate the sensitivity of the bioreactor's performance to variations in the maximum specific growth rate, stressing the need for the accurate characterization of transport phenomena and macroscopic kinetics.

This will be essential for future novel designs of bioreactor technology for SSF using AFBP substrate-based packed beds.

4. Conclusions

This work elucidates, through a preliminary experimentation design and a simplified modeling framework, the potential of *Yl2.2ab* in SSF using AFBP in a bench-scale packed-tray bioreactor. The key findings of our research include the following:

(i) The custom-designed packed-tray bioreactor, featuring a short packing length, a wall-cooling system, and forced aeration, was effective in maintaining necessary oxygen levels but faced challenges with heat transfer due to the low thermal conductivity of the AFBP-based substrate. The forced-aeration system successfully maintained adequate oxygen transport, which is critical for the metabolic activity of *Yl*2.2ab. Under the tested conditions, *Yl*2.2ab exhibited a maximum growth rate of 28.15 m_{gx} $g_{ssdb}{}^{-1}$ h^{-1} and achieved a maximum protease production of 40.10 U $g_{ssdb}{}^{-1}$ h^{-1}. The microorganism's metabolic flexibility and extremophilic characteristics were crucial for its performance in SSF, even under varying temperature conditions (40 to 49 °C) within the bioreactor.

(ii) The integration of CFD and PCSs provided valuable insights into the hydrodynamics and heat and mass transfer phenomena within the bioreactor. The sensitivity study revealed that variations in the maximum specific growth rate (μ_X) significantly impact bioreactor performance, indicating the importance of accurately characterizing transport phenomena and macroscopic kinetics for scaling-up processes.

Further research is needed to scale up the bioreactor design for industrial applications, ensuring that the transport phenomena and kinetic parameters observed at the bench scale are applicable at larger scales. To this end, mass and heat transport parameters under abiotic conditions must be determined following engineering approaches reported in the literature. In addition, the enhancement of the bioreactor's heat transfer capabilities through improved design or material selection could mitigate the challenges associated with the low thermal conductivity of the substrate. Exploring the use of *Yl*2.2ab with different AFBP-based substrates and under various environmental conditions will help to generalize the findings and expand the potential industrial applications. Finally, incorporating more sophisticated models, including real-time monitoring and control systems, could improve the accuracy and efficiency in the design, operation, and scaling-up of SSF.

Author Contributions: Conceptualization, C.O.C.-A., L.A.P.-B. and S.H.-O.; Methodology, L.A.P.-B., S.H.-O., C.O.C.-A., M.I.R.-A. and J.J.B.-F.; Software, C.O.C.-A.; Formal analysis, A.B.-N., C.O.C.-A., S.H.-O., M.I.R.-A. and J.J.B.-F.; Investigation, A.B.-N.; Resources, L.A.P.-B.; Writing original draft, L.A.P.-B. and S.H.-O.; Writing—review & editing, L.A.P.-B., S.H.-O. and C.O.C.-A.; Supervision, C.O.C.-A. and L.A.P.-B. All authors have read and agreed to the published version of the manuscript.

Funding: This research was funded by the European Union under Agreement No. 289603 through the TRANSBIO Project (Biotransformation of byproducts from the fruit and vegetable processing industry into valuable bioproducts).

Institutional Review Board Statement: Not applicable.

Informed Consent Statement: Not applicable.

Data Availability Statement: The raw data supporting the conclusions of this article will be made available by the authors on request.

Acknowledgments: A. Barrios-Nolasco thanks CONAHCyT for the postgraduate scholarship provided during his master's studies, which enabled the realization of the project associated with this research. All authors thank Juan José Cabello-Robles and José Guillermo Rivera de la Cruz for their support in the construction and modeling of the bench-scale packed-try bioreactor. All authors also express their gratitude to TRANSBIO (Biotransformation of by-products from the fruit and vegetable processing industry into valuable bioproducts)—the European Union under Agreement nº 289603—for financial support.

Conflicts of Interest: The authors declare no conflict of interest.

References

1. Coelho, M.A.Z.; Amaral, P.F.F.; Belo, I. *Yarrowia lipolytica*: An Industrial Workhorse. *Curr. Res. Technol. Educ. Top. Appl. Microbiol. Microb. Biotechnol.* **2010**, *2*, 930–940.
2. López-Flores, A.R.; Luna-Urban, C.; Buenrostro-Figueroa, J.J.; Hernández-Martínez, R.; Huerta-Ochoa, S.; Escalona-Buendía, H.; Aguilar-González, C.N.; Prado-Barragán, L.A. Efecto del pH, temperatura y fuente de proteína y carbohidratos en la producción de proteasas por *Yarrowia lipolytica* en cultivo sólido. *Rev. Mex. Ing. Quim.* **2016**, *15*, 57–67.
3. Gottardi, D.; Siroli, L.; Vannini, L.; Patrignani, F.; Lanciotti, R. Recovery and valorization of agri-food wastes and by-products using the non-conventional yeast *Yarrowia lipolytica*. *Trends Food Sci. Technol.* **2021**, *115*, 74–86. [CrossRef]
4. do Nascimento, F.V.; Lemes, A.C.; Machado de Castro, A.; Resende Secchi, A.; Zarur Coelho, M.A. A Temporal Evolution Perspective of Lipase Production by *Yarrowia lipolytica* in Solid-State Fermentation. *Processes* **2022**, *10*, 381. [CrossRef]
5. Farias, M.A.; Valoni, E.A.; Castro, A.; Coelho, M.A. Lipase Production by *Yarrowia lipolytica* in Solid State Fermentation Using Different Agro Industrial Residues. *Chem. Eng. Trans.* **2014**, *38*, 301–306.
6. Kawasse, F.M.; Amaral, P.F.; Rocha-Leão, M.H.M.; Amaral, A.L.; Ferreira, E.C.; Coelho, M.A.Z. Morphological Analysis of *Yarrowia lipolytica* under Stress Conditions through Image Processing. *Bioproc. Biosyst. Eng.* **2003**, *25*, 371–375. [CrossRef] [PubMed]
7. Huerta-Ochoa, S.; Castillo-Araiza, C.O.; Guerrero, A.R.; Prado-Barragán, A. Whole-cell bioconversion of citrus flavonoids to enhance their biological properties. *Stud. Nat. Prod. Chem.* **2019**, *61*, 335–367.
8. Ge, X.; Vasco-Correa, J.; Li, Y. Solid-State Fermentation Bioreactors and Fundamentals. In *Current Developments in Biotechnology and Bioengineering: Bioprocesses, Bioreactors and Controls*; Larroche, C., Sanromán, M.Á., Du, G., Pandey, A., Eds.; Elsevier: Amsterdam, The Netherlands, 2017; pp. 381–402.
9. Singhania, R.R.; Soccol, C.R.; Pandey, A. Application of Tropical Agro-Industrial Residues as Substrate for Solid-State Fermentation Processes. In *Current Developments in Solid-State Fermentation*; Springer: New York, NY, USA, 2008; pp. 412–442.
10. Durand, A. Bioreactor Designs for Solid State Fermentation. *Biochem. Eng. J.* **2003**, *13*, 113–125. [CrossRef]
11. Mitchell, D.A.; von Meien, O.F.; Krieger, N. Recent Developments in Modeling of Solid-State Fermentation: Heat and Mass Transfer in Bioreactors. *Biochem. Eng. J.* **2003**, *13*, 137–147. [CrossRef]
12. Mitchell, D.A.; Krieger, N. Solid-State Cultivation Bioreactors. In *Essentials in Fermentation Technology*; Springer: Cham, Switzerland, 2019; pp. 105–133.
13. Pandey, A.; Soccol, C.R.; Rodriguez-Leon, J.A.; Singh-Nee Nigam, P. *Solid State Fermentation in Biotechnology: Fundamentals and Applications*; Asiatech Publishers, Inc.: New Delhi, India, 2001; ISBN 1-87680-06-7.
14. Barrios-Nolasco, A. Diseño, Arranque y Caracterización de un Biorreactor de Charolas para Fermentación en Medio Sólido. Master's Thesis, Autonomous Metropolitan University, Mexico City, Mexico, 2015. [CrossRef]
15. Gómez-Ramos, G.A.; Castillo-Araiza, C.O.; Huerta-Ochoa, S.; Couder-García, M.; Prado-Barragan, A. Assessment of Hydrodynamics in a Novel Bench-Scale Wall-Cooled Packed Bioreactor under Abiotic Conditions. *Chem. Eng. J.* **2019**, *375*, 121945. [CrossRef]
16. Smits, J.P.; Van Sonsbeek, H.M.; Tramper, J.; Knol, W.; Geelhoed, W.; Peeters, M.; Rinzema, A. Modelling Fungal Solid-State Fermentation: The Role of Inactivation Kinetics. *Bioprocess Eng.* **1999**, *20*, 391–404. [CrossRef]
17. Szewczyk, K.W. The Influence of Heat and Mass Transfer on Solid State Fermentation. *Acta Biochim. Pol.* **1993**, *40*, 90–92. [CrossRef] [PubMed]
18. Hernández-Martínez, R.; Sancho-Solano, A.; Loera-Corral, O.; Rojo-Domínguez, A.; Regalado-González, C.; Huerta-Ochoa, S.; Prado-Barragán, L.A. Purification and characterization of a novel thermostable alkaline protease produced by *Yarrowia lipolytica*. *Rev. Mex. Ing. Quim.* **2011**, *10*, 333–341.
19. Transbio Final Report (289603). Available online: https://cordis.europa.eu/project/id/289603/reporting/fr (accessed on 22 March 2022).
20. Londoño-Hernandez, L.; Ruiz, H.A.; Ramírez, C.; Ascacio, J.A.; Rodríguez-Herrera, R.; Aguilar, C.N. Fungal detoxification of coffee pulp by solid-state fermentation. *Biocatal. Agric. Biotechnol.* **2020**, *23*, 101467. [CrossRef]
21. Dubois, M.; Gilles, K.A.; Hamilton, J.K.; Rebers, P.A.; Smith, F. Colorimetric method for determination of sugars and related substances. *Anal. Chem.* **1956**, *28*, 350–356. [CrossRef]
22. Johnvesly, B.; Naik, G.R. Studies on Production of Thermostable Alkaline Protease from Thermophilic and Alkaliphilic *Bacillus* sp. JB-99 in a Chemically Defined Medium. *Proc. Biochem.* **2001**, *37*, 139–144. [CrossRef]
23. Gratzek, J.P.; Toledo, R.T. Solid Food Thermal Conductivity Determination at High Temperatures. *J. Food Sci.* **1993**, *58*, 908–913. [CrossRef]
24. Figueroa-Montero, A. Modelamiento de la Transferencia de Calor y Masa (Agua) en un Biorreactor de Charolas para Fermentación en Medio Sólido. (Parte Uno). Doctoral Thesis, Autonomous Metropolitan University, Mexico City, Mexico, 2011. [CrossRef]
25. Choi, Y. Food Thermal Property Prediction as Effected by Temperature and Composition. Doctoral Thesis, Purdue University, West Lafayette, IN, USA, 1985.
26. Alvarado-Camacho, C.; Poissonnier, J.; Thybaut, J.W.; Castillo-Araiza, C.O. Toward the Industrial Exploitation of the Oxidative Dehydrogenation of Ethane over a NiO-SnO_2-Based Catalyst: Regime, Parametric Sensitivity, and Optimization Analysis. *Ind. Eng. Chem. Res.* **2023**, *62*, 10342–10357. [CrossRef]

27. García-Martínez, L.E.; Castillo-Araiza, C.O.; Quijano, G.; Huerta-Ochoa, S. On the modelling and surface response analysis of a non-conventional wall-cooled solid/gas bioreactor with application in esterification. *Chem. Eng. J.* **2022**, *437*, 135063. [CrossRef]
28. Hernandez-Aguirre, A.; Hernandez-Martinez, E.; López-Isunza, F.; Castillo, C.O. Framing a novel approach for pseudo-continuous modeling using Direct Numerical Simulations (DNS): Fluid dynamics in a packed bed reactor. *Chem. Eng. J.* **2022**, *429*, 132061. [CrossRef]
29. Froment, G.F.; Bischoff, K.B.; De Wilde, J. *Chemical Reactor Analysis and Design*, 3rd ed.; John Wiley & Sons: Hoboken, NJ, USA, 2010; ISBN 978-0-470-56541-4.
30. Romero-Limones, A.; Poissonnier, J.; Castillo-Araiza, C.O.; Thybaut, J.W. Avoiding false runaway prediction by properly describing axial conductive heat transfer in a low dt/dp industrial-scale packed bed reactor. *Chem. Eng. J.* **2023**, *475*, 146167. [CrossRef]
31. Tillman, D.A. *Wood as an Energy Resource*; Elsevier: Amsterdam, The Netherlands, 1978; ISBN 978-0-12-691260-9.
32. Lian, G.; Thiru, A.; Parry, A.; Moore, S. CFD Simulation of Heat Transfer and Polyphenol Oxidation during Tea Fermentation. *Comput. Electron. Agric.* **2002**, *34*, 145–158. [CrossRef]
33. Levenspiel, O. *Chemical Reaction Engineering*, 3rd ed.; John Wiley & Sons: Hoboken, NJ, USA, 1999; ISBN 047125424X.
34. De Nardi, I.R.; Zaiat, M.; Foresti, E. Influence of the Tracer Characteristics on Hydrodynamic Models of Packed-Bed Bioreactors. *Bioprocess Eng.* **1999**, *21*, 469–476. [CrossRef]
35. Rojas-Vargas, A.; Pérez, A.G. Modelación de La Curva de Distribución Del Tiempo de Residencia En Un Sistema de Lixiviación Industrial. *Tecnol. Quím.* **2009**, *29*, 213–218.
36. Ashley, V.M.; Mitchell, D.A.; Howes, T. Evaluating Strategies for Overcoming Overheating Problems during Solid-State Fermentation in Packed Bed Bioreactors. *Biochem. Eng. J.* **1999**, *3*, 141–150. [CrossRef]
37. Steele, R. *Understanding and Measuring the Shelf-Life of Food*; Woodhead Publishing: Sawston, UK, 2004; ISBN 1855737329.
38. Loera-Corral, O.; Porcayo-Loza, J.; Montesinos-Matias, R.; Favela-Torres, E. Production of Conidia by the Fungus *Metarhizium anisopliae* Using Solid-State Fermentation. In *Microbial-Based Biopesticides: Methods and Protocols*; Humana: New York, NY, USA, 2016; pp. 61–69.